Journal of Waterway, Port, Coastal, and Ocean Engineering. Submitted November 28, 2012; accepted May 2, 2013; posted ahead of print May 4, 2013. doi:10.1061/(ASCE)WW.1943-5460.0000209

A comprehensive field study of swash-zone processes, Part 2: Sheet flow sediment concentrations during quasi-steady backwash

Submitted to the Journal of Waterway, Port, Coastal, and Ocean Engineering

Thijs Lanckriet[1], Jack A. Puleo[2], Gerd Masselink[3], Ian L. Turner[4], Daniel Conley[5], Chris Blenkinsopp[6] and Paul Russell[7]

[1]Graduate Assistant, Center for Applied Coastal Research, Department of Civil and Environmental Engineering, University of Delaware, Newark, DE 19716 (corresponding author). E-mail: thijs@udel.edu

[2]Associate Professor, Center for Applied Coastal Research, Department of Civil and Environmental Engineering, University of Delaware, Newark, DE 19716. E-mail: jpuleo@udel.edu.

[3]Professor, Coastal Processes Research Group, School of Marine Science and Engineering, Plymouth University, Plymouth, PL4 8AA, UK. E-mail: gerd.masselink@plymouth.ac.uk.

[4]Associate Professor, Water Research Laboratory, School of Civil and Environmental Engineering, University of New South Wales, Manly Vale, NSW 2093 Australia. E-mail: ian.turner@wrl.unsw.edu.au

[5] Associate Professor, Coastal Processes Research Group, School of Marine Science and Engineering, Plymouth University, Plymouth, PL4 8AA, UK. E-mail: daniel.conley@plymouth.ac.uk

[6]Lecturer, Water Research Laboratory, School of Civil and Environmental Engineering, University of New South Wales, Manly Vale, NSW 2093 Australia. E-mail: c.blenkinsopp@wrl.unsw.edu.au

[7]Professor, Coastal Processes Research Group, School of Marine Science and Engineering, Plymouth University, Plymouth, PL4 8AA, UK. E-mail: paul.russell@plymouth.ac.uk

Abstract

Sheet flow sediment concentration profiles were measured in natural conditions for the first time as part of a comprehensive field study on swash-zone hydrodynamics and sediment transport. Three conductivity concentration profilers (CCPs) measured the sediment concentration profile in the sheet flow layer with a 1 mm resolution in the swash zone of a dissipative beach. This paper focuses on sheet flow during quasi-steady backwash events generated by infragravity motion when the effects of phase lags, surface-generated turbulence and accelerations are small. The sheet flow sediment concentration profile has a linear shape in the lower section of the profile and a power-law shape in the upper section, with the transition occurring at sediment volume fractions of 0.20-0.30. The shape of the concentration profile is self-similar for measured sheet flow layer thicknesses ranging from 6 mm to 18 mm. Because of the self-similarity, a single concentration profile curve can be used to describe the normalized profile for the entire range of sheet thicknesses, leading to improved estimates of the sheet flow layer thickness in a simple analytical model. The sheet flow layer thickness and sheet load, the sediment mass mobilized in the sheet flow layer, are well-correlated with the hydrodynamic forcing represented by the mobility number ($r^2 = 0.60$ for sheet thickness and $r^2 = 0.53$ for sheet load).

Keywords: swash zone, sheet flow, sediment transport, beach face, sandy beach

Journal of Waterway, Port, Coastal, and Ocean Engineering. Submitted November 28, 2012; accepted May 2, 2013; posted ahead of print May 4, 2013. doi:10.1061/(ASCE)WW.1943-5460.0000209

Introduction

Sheet flow is believed to contribute significantly to nearshore sediment transport and considerable progress in the understanding of this process has been gained through laboratory and numerical studies. However, sheet flow sediment transport is more difficult to measure directly in natural environments than suspended load transport. The swash zone in particular is an area where sheet flow is speculated to represent a significant fraction of the total sediment transport and where the overall understanding of sediment transport mechanisms is still weak. New measurement techniques now make it possible for the first time to directly measure detailed sheet flow sediment concentration profiles in the swash zone under natural conditions and test existing knowledge of sheet flow dynamics.

The first measurements of unidirectional sheet flow were conducted in annular, parallel-plate shear cells (Bagnold 1954; Savage and Mckeown 1983; Hanes and Inman 1985) and provided constitutive relationships for the grain stresses that are the mobilizing mechanism for sheet flow. Experiments in recirculating flow tunnels (Shook et al. 1982; Sumer et al. 1996; Pugh and Wilson 1999) provided additional insights into the velocity and sediment concentration profiles in the sheet flow layer and the increased bed roughness due to sheet flow. Sheet flow measurements under sinusoidal, asymmetric and irregular forcing were conducted in oscillatory flow tunnels (Horikawa et al. 1982; Ribberink and Al-Salem 1995; Dibajnia and Watanabe 1998; Dohmen-Janssen et al. 2001; Ahmed and Sato 2003; O'Donoghue and Wright 2004b; Ribberink et al. 2008; van der A et al. 2010; Capart and Fraccarollo 2011; Ruessink et al. 2011; Dong et al. 2013). These studies have established thresholds for the transition between the ripple regime and the sheet flow regime, and have provided the most detailed sediment concentration and velocity profiles in the sheet layer to date. Oscillatory flow tunnel studies also elucidated the relationship between velocity and acceleration asymmetry, phase lags between the free-stream velocity, bed shear stress and mobilized sediment, and the net sediment flux. Studies in large-scale wave flumes provide a more realistic reproduction of the coastal environment and add the effects of free surface flow such as boundary layer streaming, which alters the net transport rate (Dohmen-Janssen and Hanes 2002, 2005; Schretlen et al. 2010). Numerical models yield additional insights into the sheet flow process, but require validation by physical experiments (Hsu et al. 2004; Calantoni and Puleo 2006; Amoudry et al. 2008; Bakhtyar et al. 2009; Yu et al. 2010; Chen et al. 2011).

Measurements of sheet flow under natural conditions have been scarce, mainly due to the difficulty of capturing the high-concentration sheet layer near the sediment bed which may experience bed level changes that are larger than the thickness of the sheet layer over short lengths of time (Blenkinsopp et al. 2011b). Since sheet flow is believed to occur frequently in the near-shore (Nielsen 1992), this lack of measurements forms an obstacle to a complete understanding of near-shore sediment transport. Particularly in the swash zone, where large sediment fluxes occur in small water depths, near-bed and sheet flow transport may account for a large fraction of the total sediment transport (Masselink and Puleo 2006).
Bakker et al. (1988) and Yu et al. (1990) provided the only known field measurements in the swash-zone sheet flow layer to date, in contrast with the large number of swash-zone field studies that focused on suspended load (e.g., Osborne and Rooker 1999; Butt and Russell 1999; Puleo et al. 2000; Masselink et al. 2005; Hughes et al. 2007; Cáceres and Alsina 2012).

Journal of Waterway, Port, Coastal, and Ocean Engineering. Submitted November 28, 2012; accepted May 2, 2013; posted ahead of print May 4, 2013. doi:10.1061/(ASCE)WW.1943-5460.0000209

A Conductivity Concentration Profiler (CCP) instrument was recently developed with the specific aim of providing sediment concentration profile measurements in the sheet flow layer in field and large-scale laboratory settings (Lanckriet et al. 2013). The first field deployment of the CCP took place during a field study on swash-zone hydrodynamics and sediment transport in Perranporth, UK. Infragravity wave motion on this dissipative beach generated long-duration backwash events in which the flow gradually accelerated, creating a quasi-steady hydrodynamic forcing for the sheet flow layer. This quasi-steady backwash sheet flow is the least complicated case of sheet flow in the swash zone since surface-generated turbulence, inertial and phase lag effects are small, making it an appropriate starting point to investigate sheet flow under field conditions and validate existing knowledge on sheet flow processes.

The BeST (Beach Sand Transport) field study, conducted from 9 to 15 October 2011 at Perranporth Beach, Cornwall, UK, had the objective of collecting a complete dataset of swash zone hydrodynamics and sediment transport under field conditions. Part 1 of this contribution provided an overview of the field study, including a detailed description of the field site and the suite of deployed instruments (Puleo et al. this issue). Part 1 also presented representative time series of morphodynamic, hydrodynamic and sediment processes. Part 2 provides a detailed description of the sheet flow sediment concentration profile measurements during quasi-steady backwash. First, a brief summary of the study site and instrumentation is given. Next, results of the sediment concentration measurements are presented, focusing on four aspects: 1) the sediment concentration profile shape, 2) the sheet flow layer thickness, 3) the sheet load, which is the amount of sediment mobilized within the sheet layer and 4) the relationship between hydrodynamic forcing, sheet flow layer thickness and sheet load. Then, a discussion of the results highlights implications for an existing derivation of the sheet flow layer thickness, followed by conclusions.

Methodology

Study site

The field site is a macrotidal, dissipative beach facing west-northwest and is enclosed between two headlands that are separated by approximately 3.5 km. The median grain diameter in the vicinity of the instruments d_{50} was 0.33 mm. Measurements were taken for approximately 3 hours around high tide for 10 consecutive tidal cycles. Initial high tide measurement cycles were used to test the CCP instruments and optimize the sensor positioning. Only measurements from three high tides (Tides 7-9), taken during 13 and 14 October, are discussed in this paper. Offshore wave conditions are summarized in Table 1. The beach slope around the main instrument bar, located near the spring high tide water level, evolved from 1:41 to 1:46 over the course of the three high tides, although the slope was generally flatter on the more seaward-located section of the intertidal beach. Maximum uprush velocities were 2.05 – 2.35 m/s; peak backwash velocities reached -1.79 – -2.19 m/s for the three high tide cycles.

Instrumentation

A 45-meter long scaffold rig was erected across the high-tide swash zone containing a suite of instruments. Only measurements made by instruments on the main instrument bar, located 7.4 m from the

Journal of Waterway, Port, Coastal, and Ocean Engineering. Submitted November 28, 2012; accepted May 2, 2013; posted ahead of print May 4, 2013. doi:10.1061/(ASCE)WW.1943-5460.0000209

seaward edge of the scaffold rig, are discussed in this paper. Velocities were recorded using two Valeport electromagnetic current meters (EMCMs) that were positioned 0.03 m and 0.06 m above the bed, and water levels were measured using a pressure transducer (Druck PTX1830) buried 0.05 m beneath the bed.

Sediment concentrations in the sheet flow layer were recorded using three Conductivity Concentration Profilers (CCPs; Lanckriet et al. 2013) spaced by approximately 0.2 m in the alongshore and directly beneath the main instrument bar (Fig. 1). Using electrical conductivity as a proxy for sediment concentration, the CCP renders a 29-point vertical concentration profile with a 1 mm resolution for sediment volume fractions ranging from 0.05 to a packed sediment bed (volume fractions of approximately 0.644; Bagnold 1966). The response between conductivity and concentration has been validated by Lanckriet et al. (2013) with laboratory measurements of sand suspended neutrally in a Lithium Metatungstate heavy liquid, and agreed well with Archie's law (Archie 1942):

$$\frac{\sigma_m}{\sigma_f} = (1-c)^m \ , \tag{1}$$

where σ_f is the conductivity of the fluid in the absence of sediment, σ_m is the conductivity of the sediment-fluid mixture, c is the sediment volume fraction and m is a calibration factor that is determined by sediment characteristics such as grain size and shape. Field measurements by the CCPs were calibrated by determining the clear-water conductivity σ_f from measurements high in the water column, where sediment volume fractions are negligible, for each high tide to account for variations in the water conductivity between different high tides, e.g., due to potential salinity and temperature changes. The calibration factor m was determined based on measurements in the immobile sediment bed below the sheet flow layer, assuming a packed-bed concentration of 0.644 (Bagnold 1966). A single value for m was determined for all three high tides to obtain a more robust estimate since sediment characteristics remained constant between high tide cycles. Measured concentration profiles are smoothed in the CCP measurement process due to the finite size of the measurement volume of the CCP, increasing the measured sheet thickness. Lanckriet et al. (2013) studied the smoothing effect in detail by simulating the electric field around the CCP probe using a finite difference model and developed a correction formula for the sheet layer thickness to account for the smoothing effect. For this reason, the sheet flow layer can only be resolved by the CCP when the sheet flow layer thickness, determined according to the procedure described in the following section, is larger than 5 mm.

The CCPs, with a vertical measurement window of 29 mm, were positioned at vertical elevations offset by approximately 15 mm to capture the sheet layer processes under active bed accretion or erosion while still providing overlap between profiles measured by different sensors. Occasionally one or more of the three co-located CCP probes remained buried under the sheet flow layer or remained exposed in the water column above the sheet flow layer due to significant bed level changes that intermittently occurred during individual swash events. Since bed-level changes over the monitored tides were limited to O(10 mm), the sheet layer was captured by one or two CCP instruments during all three high tides. Flow disturbance and potential scour

Journal of Waterway, Port, Coastal, and Ocean Engineering. Submitted November 28, 2012; accepted May 2, 2013; posted ahead of print May 4, 2013. doi:10.1061/(ASCE)WW.1943-5460.0000209

under field deployment were minimized by the small cross-sectional area of the conductivity probe (1.6 mm thickness; 5.6 mm width) and by burying the sensor electronics housing in the inactive sediment bed. The EMCMs, pressure transducers and CCPs all sampled at 4 Hz and were recorded on a bank of computers that were time-synchronized to a GPS clock, but the sampling itself was not triggered simultaneously across different instruments. Therefore, all measurements were interpolated onto a common discrete time series with intervals of 0.25 s.

Measurements quality control

To ensure the quality of the sediment concentration profile measurements made by the CCP, measurements were discarded if any of the following conservative criteria were met:

- Sheet flow occurred with a sheet layer thickness smaller than 5 mm as this cannot be accurately resolved by the CCP.
- The angle of the flow velocity vector relative to shore normal exceeded 15°. Flow angle time series were determined using the lower EMCM velocity measurements. This criterion ensured that the flow was nearly shore-normal and thus roughly parallel to the CCP probe. As the probe is 1.6 mm thick and 5.6 mm wide, flow disturbance and scour will be insignificant when the flow is aligned with the sensor. Under oblique flow, eddy shedding and scour may occur near the sensor, altering the sheet flow layer near the sensor. When the water level was below the lowest current meter, no velocities and no flow angle could be determined. In this case, CCP measurements were discarded for lack of a reliable velocity signal even though it is believed that the CCP still accurately captures sheet flow sediment concentrations during these instances.
- The 15 minutes following the first bore arrival during rising tide were discarded to allow the sand bed to compact and fully saturate around the CCP probes.
- When two collocated CCPs both recorded the entire sheet layer within the profiling window and the calculated sheet thickness differed by more than 4 mm, the measured sheet thickness was discarded.

Over the three high tide measurement periods defined in Table 1, CCP measurements were made for a total of 94765 sampling instances (6.5 hours). Sheet flow with a thickness of 5 mm or more was recorded for 25199 sampling instances (112 minutes). 69 % of these measurement instances occurred under oblique flow or when no current meter data were available, 3 % occurred during the first 15 minutes of each high tide cycle and CCP sheet thicknesses disagreed by more than 4 mm for 2 %. As a result, 7416 sampling instances (31 minutes) passed all quality control criteria. Two CCPs recorded the sheet flow layer simultaneously during many of these instances leaving 10082 sediment concentration profiles that passed the quality control criteria.

The least complex swash-zone sheet flow sediment transport conditions occur under quasi-steady backwash when effects from bore-generated turbulence, pressure gradients and phase lags are negligible. Quasi-steady backwash conditions were defined when all of the following criteria were met:

- The velocity as measured by the lowest EMCM was offshore-directed.

Journal of Waterway, Port, Coastal, and Ocean Engineering. Submitted November 28, 2012; accepted May 2, 2013; posted ahead of print May 4, 2013. doi:10.1061/(ASCE)WW.1943-5460.0000209

- Fluid accelerations were small. A threshold for accelerations was defined as $\frac{dU}{dt} < 1.2\, g \sin\gamma = 0.27\, m/s^2$, where γ is the beach slope, g is gravitational acceleration, and U is the flow velocity magnitude measured by the lowest EMCM. Swash flow during the backwash initially accelerates under gravity and the acceleration decreases at the end of the swash cycle when the gravitational force is balanced by bottom friction (Hughes and Baldock 2004). Acceleration effects are assumed to be small when the flow accelerates under gravity on a low-sloping beach. The acceleration threshold used here is an order of magnitude smaller than peak accelerations in oscillatory flow tunnel studies (e.g., $\left(\frac{dU}{dt}\right)_{max} = 1.33 - 2.00$ in O'Donoghue and Wright 2004b; $\left(\frac{dU}{dt}\right)_{max} = 1.47 - 1.87$ in Ruessink et al. 2011) and corresponds to a modified Sleath number S (Foster et al. 2006)

$$S = \frac{\frac{dU}{dt}}{(s-1)g} = 0.017, \tag{2}$$

  where $s = 2.65$ is the relative density of the sediment. This Sleath number is an order of magnitude smaller than the limit for pressure gradient-induced sediment mobilization (Sleath 1999; Foster et al. 2006).
- Abrupt water depth changes were occasionally recorded by the pressure transducer during the backwash when no acceleration was registered. This may either be caused by a small secondary wave propagating onshore during a backwash, or when a new bore arrived at the sensor location and initiated a new uprush event while the near-bed flow velocity was still offshore-directed. These events were excluded by discarding all measurements when $\frac{dh}{dt} > 0.05\, m/s$.
- If the acceleration and water depth thresholds were exceeded for a particular record, data from 0.75 s before until 0.25 s after the measurement were also removed from the time series since a sudden acceleration or bore may stir up sediment that stays mobilized during later times and to account for small timing differences between the different instruments.

5313 measurements were taken during backwash events (22 minutes). 22% of these measurements were rejected due to accelerations and 14% because of water depth changes. As a result, a total of 3863 measurements were taken during quasi-steady backwash (16 minutes). Again, the sheet layer was measured by two CCPs during some of these instances, resulting in a total of 5365 profiles.

Journal of Waterway, Port, Coastal, and Ocean Engineering. Submitted November 28, 2012; accepted May 2, 2013; posted ahead of print May 4, 2013. doi:10.1061/(ASCE)WW.1943-5460.0000209

Results

A time series excerpt is displayed in Fig. 2. Multiple swash events occurred with gravity-timescale bores superimposed on infragravity-timescale swash cycles with a maximum depth of 0.22 m. The flow direction alternated multiple times between onshore (uprush) and offshore (backwash) within a single infragravity swash cycle in conjunction with the gravity-timescale bores. Cross-shore and alongshore velocities are displayed in Fig. 2b, with the cross-shore velocity displayed as a thick black curve for times when quasi-steady sheet flow occurred that met all quality control criteria.

Sediment concentration measurements (Fig. 2c) demonstrate that the sediment bed is active throughout most of the swash event, with the immobile bed level (black line) nearly continuously changing as a result of local hydrodynamic forcing and cross-shore and alongshore sediment transport gradients. Black and magenta lines indicate the top and bottom boundary of the sheet flow layer as defined in the following section. Smoothing of the sediment concentration profile by the CCP instrument (see previous section) causes the top and bottom boundary to appear to be separated by approximately 4-5 mm when the bed is at rest and no sheet flow layer is present, which was the case during gradual flow reversals (e.g., at 17:30:03 UTC and 17:30:52 UTC). A method to correct for the smoothing effect on sheet thickness estimates based on Lanckriet et al. (2013) is described in the following section.

When the top and bottom boundaries of the sheet flow layer (black and magenta lines in Fig. 2c) are separated by more than 5 mm, sediment is considered to be mobilized as sheet flow. Sheet flow under quasi-steady backwash conditions occurred for 5 quality-controlled backwash events during this time segment, highlighted by thick black lines in Fig. 2b. Some backwash flows, e.g., at 17:30:30-17:30:41 UTC, contained a strong alongshore component, resulting in flows oblique to the CCP probe and sheet thicknesses were discarded during these instances. During other instances, such as at 17:31:01-17:31:06, the backwash flow was too shallow to be recorded by the lowest current meter, meaning that flow angle could not be determined. Instantaneous sediment concentration profiles are displayed in Fig. 2d-g for 4 backwash sheet flow events indicated by yellow vertical lines in Fig. 2c. Two collocated CCPs measured the sediment concentration in the sheet flow layer during these events. The agreement between sediment concentration profiles measured by the two collocated sensors (black solid line and blue dotted line in Fig. 2d-g) indicates repeatability of the measurements.

Concentration profile

Top and bottom boundary of the sheet layer

The top boundary of the sheet flow layer is typically defined as the location where grains become (on average) separated enough so that intergranular forces become negligble. Bagnold (1956) defines the top boundary at the volume fraction where the mean radial separation distance between grains equals one grain diameter, $\lambda = 1$, equivalent to a sediment volume fraction c of 0.08. Therefore, $c = 0.08$ was chosen as the cut-off concentration for the top of the sheet flow layer, similar to previous sheet flow sediment transport studies (Dohmen-Janssen and Hanes 2002; O'Donoghue and Wright 2004a).

Journal of Waterway, Port, Coastal, and Ocean Engineering. Submitted November 28, 2012; accepted May 2, 2013; posted ahead of print May 4, 2013. doi:10.1061/(ASCE)WW.1943-5460.0000209

The bottom boundary of the sheet flow layer, the boundary between the sheet flow layer and the non-moving sediment bed, is more difficult to define since the concentration of the non-moving sediment bed varies over time under field conditions. Sediment that is packed at the closest packing limit, around c = 0.644 for natural sands (Bagnold 1966), is immobile by definition. Sediment that is packed at a concentration between the closest packing limit and the loosest packing limit may be mobile or immobile since it is packed densely enough to support itself statically, but loosely enough to allow sediment motion. Moreover, the loose packing fraction is difficult to determine experimentally and is not as well-established as the random close-packing limit. The loose packing limit is approximately c = 0.55 for uniform spheres (Song et al. 2008), but may be less for natural sands. Bagnold (1966) found c = 0.51 for beach sand, and Baker and Kudrolli (2010) found c = 0.50-0.54 for platonic solids which, like natural sand, are angular, lowering the random loose packing limit. A simple approach to defining the bottom of the sheet flow layer was applied in a preliminary analysis of the field measurements presented here where the bottom was defined as the location where the smoothed measured concentration profile exceeds the loose packing limit, $c = 0.51$ (Lanckriet et al. 2013). Although this approach yields satisfying results for the profiles displayed in Fig. 3, it produced many estimates for the bottom of the sheet layer that were clearly too low in other locations of the dataset. What is obvious is that a simple criterion based on c is unlikely to work, and a more sophisticated methodology for determining the bottom of the sheet flow layer is required.

Yu et al. (2012) divided the sheet flow layer into two parts: an upper layer of 'rapid sediment flow' with $c_l < c < c_t$ and a lower layer with $c_c < c < c_l$, where $c_t = 0.08, c_l = 0.57$ and $c_c = 0.635$ are the concentration at the top of the sheet layer, the random loose packing concentration and the random close packing concentration, respectively. In the lower layer, grains are in enduring contact and the flow behaves like a glassy solid. Experimental results by Capart and Fraccarollo (2011) display a similar division of the sheet flow layer into two sublayers. Results from a 1DV, two-phase numerical model based on this division show that the total sediment transport in the lower layer is smaller [O(10%)] than in the upper layer for unidirectional, sinusoidal and skewed oscillatory flow, and that there is a sharp 'shoulder' transition in the concentration profile between the two layers (Amoudry et al. 2008; Yu et al. 2010). This shoulder is also observed in measured sheet flow sediment concentration profiles (O'Donoghue and Wright 2004a; Dohmen-Janssen and Hanes 2005). Since the shoulder is also observed in sediment concentration profiles measured by the CCP, it was used to define the bottom of the sheet layer using a technique similar to O'Donoghue and Wright (2004a). This means that the glassy lower region of the sheet flow layer, and the small fraction of the total sheet flow transport that may take place in this layer, was ignored.

Instantaneous concentration profiles for two of the backwash sheet flow events discussed earlier are displayed in Fig. 3 to illustrate the method to determine the top and bottom boundaries of the sheet flow layer. To determine the top boundary of the sheet flow layer, the instantaneous profile (Fig. 3 black lines) is smoothed spatially using a boxcar average with a width of 3 mm (3 points in the profile) and the top of the sheet layer is defined as the elevation where the smoothed concentration profile equals 0.08 (red upward-facing triangles in Fig. 3).

Journal of Waterway, Port, Coastal, and Ocean Engineering. Submitted November 28, 2012; accepted May 2, 2013; posted ahead of print May 4, 2013. doi:10.1061/(ASCE)WW.1943-5460.0000209

The sharp shoulder transition in the sheet flow concentration profiles was observed in both profiles at volume fractions between 0.51 and 0.55 (Fig. 4). The method used to define the bottom boundary of the sheet flow layer is based on O'Donoghue and Wright (2004a) who fitted a curve to the sheet flow sediment concentration profile of the form:

$$\breve{c}(z) = \frac{\beta^{\alpha}}{\beta^{\alpha} + [z - z_1]^{\alpha}} , \tag{3}$$

where $\breve{c}(z)$ is the instantaneous sediment concentration profile normalized by the sediment concentration in the packed bed, z_1 is the first estimate of the bottom of the sheet flow layer, and α and β are fitted shape parameters. Since the concentration in the packed bed varies under field conditions, a curve of the following form is used instead (referred to hereafter as the ODW curve):

$$c(z) = c_b \frac{\beta^{\alpha}}{\beta^{\alpha} + [z - z_1]^{\alpha}} , \tag{4}$$

where c_b is the concentration in the bed, determined by fitting (4) to each of the instantaneous concentration profiles with α, β, c_b and z_1 as free parameters. O'Donoghue and Wright (2004a) found that due to the shape of this curve, the estimated bottom of the sheet layer z_1 is sometimes too low and this is also seen in the curves in Fig. 3 (blue circles). Therefore, they extended a straight line through the inflection point of the curve (red diamond in Fig. 3) and defined an improved estimate of the bottom of the sheet layer, z_e, as the intersection of the straight line with the bed concentration c_b (down-facing triangle). For the profiles displayed in Fig. 3, the elevation z_e of the new estimate for the bottom of the sheet layer agrees well with the location of the shoulder in the profile and z_e was therefore chosen as the bottom of the sheet flow layer. Defining the bottom of the sheet flow layer by extending the linear portion of the sheet flow concentration profile is similar to the method used by Pugh and Wilson (1999).

The sheet flow layer thickness δ_s was defined for each individual profile as the vertical distance between the top and bottom boundary of the sheet flow layer. Additionally, the sediment volume mobilized within the sheet flow layer, or volumetric sheet load, was determined as

$$\Phi = \int_{z_e}^{z_t} c \, dz \ . \tag{5}$$

The sediment mass mobilized in the sheet layer, or sheet load, was then defined as

$$\mathrm{C} = \rho_s \Phi \ , \tag{6}$$

Journal of Waterway, Port, Coastal, and Ocean Engineering. Submitted November 28, 2012; accepted May 2, 2013; posted ahead of print May 4, 2013. doi:10.1061/(ASCE)WW.1943-5460.0000209

where $\rho_s = 2650 kg/m^3$ is the sediment mass density.

Sheet thickness estimates must be corrected for the smoothing of the concentration profile introduced by the CCP measurement process. The correction formula by Lanckriet et al. (2013) was based on a numerical model of the electric field around the CCP. A simplified sheet layer with a piecewise linear concentration profile was simulated and the top and bottom of the sheet layer were defined using cut-off values in the conductivity profile. Analysis of the CCP field measurements has shown that using a concentration or conductivity cut-off for the bottom of the sheet layer leads to errors and this has led to the method described in this section to determine the bottom of the sheet layer. Therefore, the numerical simulations were reanalyzed to adjust the correction factor to this new definition of the top and bottom of the sheet layer. The top and bottom of the simulated sheet layer were determined using the curve-fitting method described above, and a new correction formula then removes the smoothing effect from the measured sheet thickness values:

$$\frac{\delta_{sens}}{\delta_{real}} = \frac{1}{713 \cdot 10^3 \delta_{sens}^2 - 6024 \delta_{sens} + 21.9} + 1, \tag{7}$$

with δ_{real} and δ_{sens} the real sheet thickness (without smoothing) and measured thickness by a CCP sensor (including smoothing) respectively, expressed in meters. Based on this new analysis, the minimum sheet thickness that can be resolved by the CCP is 5 mm, larger than the minimum sheet thickness of 3.5 mm estimated by Lanckriet et al. (2013).

Additionally, the volumetric sheet load Φ was calculated for both the simulated CCP sensor and the prescribed sheet layer for each of the numerical simulations, and a correction formula was developed to correct the volumetric sheet load for the smoothing effect:

$$\frac{\Phi_{\text{sens}}}{\Phi_{\text{real}}} = \frac{1}{713 \cdot 10^3 \Phi_{sens}^2 - 6024 \Phi_{sens} + 21.9} + 1, \tag{8}$$

where Φ_{real} and Φ_{sens} are the real volumetric sheet load and measured volumetric sheet load, respectively.

Ensemble-averaged sediment concentration profiles

Sediment concentration profiles under quasi-steady backwash conditions were grouped according to the measured sheet thickness in 1 mm bins. Individual profiles were centered around the elevation where the concentration of the smoothed individual profile (using a 3-point boxcar average) equals 0.30 to align profiles in the vertical. Other methods, such as centering profiles around the top or bottom of the sheet layer, or the mean elevation of the top and bottom, resulted in a larger spread of the individual profiles. Using the centered, non-smoothed individual profiles, an ensemble-averaged profile was calculated for each sheet flow layer thickness. The average concentration at a particular elevation of the ensemble-averaged profile was only retained if at least one third of all individual profiles had a valid concentration measurement at that elevation.

Journal of Waterway, Port, Coastal, and Ocean Engineering. Submitted November 28, 2012; accepted May 2, 2013; posted ahead of print May 4, 2013. doi:10.1061/(ASCE)WW.1943-5460.0000209

Ensemble-averaged profiles for sheet thicknesses of 6 mm, 11 mm and 16 mm are displayed in the left, middle and right columns of Fig. 4 respectively.

Qualitatively, the bin-averaged profiles appear linear in the lower part of the sheet flow layer and have a power-law tail toward the top of the sheet flow layer, particularly for larger sheet thicknesses (Fig. 4c,f,i), in agreement with past studies (Sumer et al. 1996; Pugh and Wilson 1999). The measured sediment concentration in the non-moving sediment bed (z-$z_e < 0$) shows variability of O(0.10). Laboratory measurements in a packed sediment bed demonstrated that instrument measurement accuracy is on the order of 0.03 (Lanckriet et al. 2013, Fig. 6b). The variability observed in Fig. 4 is therefore likely because the upper layer of the non-moving bed was deposited by natural wave-induced sediment transport and is constantly reworked by shear, erosion and deposition throughout the high tide measurement cycle. For sheet thicknesses of 6 mm and 11 mm, the concentration appears to increase monotonically in the bed. This is likely due to the fact that the sand is initially deposited loosely and is subsequently packed down by the weight of sediment deposited above. As with the individual concentration profiles, the top of the sheet layer z_t was again determined as the elevation where the ensemble-averaged concentration profile, smoothed using a 3-point boxcar average, equaled 0.08. The bottom of the sheet layer z_e and the concentration in the bed c_b were first determined by fitting a curve of the form (4) to the bin-averaged profile and extending the curve from the inflection point to the bed concentration to determine the bottom of the sheet layer z_e, as was done for the individual concentration profiles. This determined the top and bottom of the sheet flow layer, the sheet flow layer thickness and the concentration in the bed.

Past work has suggested different shapes for the sediment concentration profile in the sheet layer. Several of these shapes, along with newly proposed shapes, were compared to the ensemble-averaged measured profiles. First, a linear profile has been proposed (Hanes and Bowen 1985; Wilson 1987)

$$c(z) = a_1 z + a_2, \tag{9}$$

where a_1 and a_2 are fitting parameters. Secondly, a power law has also been proposed as a shape for the concentration profile in the sheet layer (Ribberink and Al-Salem 1994)

$$c(z) = b_1 (z')^{b_2}, \tag{10}$$

where b_1 and b_2 are fitting parameters and $z' = z - z_e$ is the elevation above the bottom of the sheet layer. Third, Sumer et al. (1996) and Pugh and Wilson (1999) stated that the profile had a linear shape in the lower section of the layer and a power law tail at the upper section, defined here as a composite profile:

Journal of Waterway, Port, Coastal, and Ocean Engineering. Submitted November 28, 2012; accepted May 2, 2013; posted ahead of print May 4, 2013. doi:10.1061/(ASCE)WW.1943-5460.0000209

$$c(z) = \begin{cases} d_1\left(z' - z_{transition}\right) + c_{transition} & ,z' \le z_{transition} \\ c_{transition}\left(\dfrac{z'}{z_{transition}}\right)^{d_2} & ,z' > z_{transition} \end{cases} \tag{11}$$

where d_1 and d_2 are fitting parameters, $z_{transition}$ is the elevation above the bottom of the sheet layer where the profile transitions from a linear to a power law shape and $c_{transition}$ is the concentration at $z_{transition}$.

Fourth, O'Donoghue and Wright (2004a) proposed a curve of the form (4). The ODW curve can be rewritten in terms of the sheet thickness δ_s instead of a generic length scale β:

$$c = c_b \frac{1}{1 + \left(\dfrac{z'}{\delta_s}\right)^{\alpha} \dfrac{c_b - c_t}{c_t}}, \tag{12}$$

where $c_t = 0.08$ is the concentration at the top of the sheet layer.

Each of these curves was fitted between the top and bottom boundary of the sheet flow layer. For each shape, the goodness of fit was evaluated using the coefficient of determination R^2, defined as

$$R^2 = 1 - \frac{\sum_i \left(c_i - \overline{c}\right)^2}{\sum_i \left(c_i - c_i\right)^2}, \tag{13}$$

where c_i are the discrete concentration values in the ensemble-averaged profile, $\overline{c}$ is the mean of all concentration values c_i in the ensemble-averaged profile, and c_i are the values predicted by the curve fit. Results for all fitted shapes are summarized in Table 2.

The linear fit (red dotted line, Fig. 4a,b,c) describes the sheet layer relatively well for small sheet thicknesses. For larger sheet layers, however, the discrepancy between the concentration profile and the linear fit increases as the power-law tail at the top of the sheet layer becomes more prominent. The coefficient of determination R^2 thus decreases from 0.97 for small sheet layer thicknesses to 0.87 for large thicknesses. The power law is not a satisfactory description for the sheet layer down to the non-moving bed ($0.61 \le R^2 \le 0.90$) because the concentration diverges to infinity as $z' \to 0$ for a concentration profile that decays away from the bed (exponent $b < 0$).

The composite profile (Fig. 4d,e,f) provides a near-perfect fit for all sheet layer thicknesses ($R^2 > 0.99$). The transition point between the linear and power-law segment was chosen so that the overall composite profile had the maximum coefficient of determination R^2, making it possible to determine where the profile

Journal of Waterway, Port, Coastal, and Ocean Engineering. Submitted November 28, 2012; accepted May 2, 2013; posted ahead of print May 4, 2013. doi:10.1061/(ASCE)WW.1943-5460.0000209

transitions from a linear to a power-law shape. The concentration profile transitions to a power-law shape at concentrations in the range 0.20 – 0.30 and at elevations of 0.27 δ_s - 0.57 δ_s (Table 2). The results are not sensitive to the location of the transition point so the elevation of the transition point (and the associated concentration) can be changed by several millimeters without significantly reducing the goodness of fit.

The ODW curve expressed as eq. (12) was fitted to the data with the sheet thickness δ_s and the concentrations at the top and bottom of the sheet layer, c_b and c_t, all held fixed, and with the shape parameter α as the only free parameter, resulting in an excellent fit to the ensemble-averaged concentration profiles ($R^2 \geq 0.98$). The shape parameter α varied between 1.44 and 2.03, in good agreement with the range of values for α = 1.1-1.9 found by O'Donoghue and Wright (2004a) for time-averaged profiles in oscillatory flows. The small range of values for □ indicates a high level of similarity between ensemble-averaged sediment concentration profiles of varying thickness. Therefore, a second ODW curve was compared to the data with □ held constant at 1.73, the mean value across all sheet thicknesses. This curve again agreed well with the ensemble-averaged profiles (R 2≥ 0.94; red dotted line in Fig. 4g,h,i).

The ODW shape is similar to the composite linear-power law profile because the ODW curve has an inflection point, making the curve locally linear in the lower section of the sediment concentration profile, and it reduces to a power law for □ →∞. The only difference with the composite profile is that the transition between linear and power-law behavior occurs smoothly in the case of the ODW. The finding that □ varies relatively little in the ODW curves with □ as a fitting parameter indicates that there is a high level of self-similarity between sheet flow sediment concentration profiles of varying sheet thickness. This self-similarity is demonstrated in Fig. 6, in which all 5365 individual profiles are displayed, scaled by their sheet thickness so that the vertical coordinates equal 0 and 1 at the bottom and top of the sheet flow layer, respectively. The solid black curve indicates the ensemble average of all normalized profiles.

Sheet thickness and sheet load

Hydrodynamic forcing for unidirectional sheet flow is typically described using the Shields number θ:

$$\theta = \frac{\tau_b}{\rho_f (s-1) g d} \tag{14}$$

or the mobility number ψ:

$$\psi = \frac{U^2}{(s-1) g d}, \tag{15}$$

where τ_b is the bed shear stress, ρ_f is the fluid density and d is a representative grain diameter which is typically defined as the median grain diameter d_{50}.

Journal of Waterway, Port, Coastal, and Ocean Engineering. Submitted November 28, 2012; accepted May 2, 2013; posted ahead of print May 4, 2013. doi:10.1061/(ASCE)WW.1943-5460.0000209

Wilson (1987) proposed a linear relationship between the sheet thickness δ_s and the Shields number:

$$\frac{\delta_s}{d} = \Lambda\theta\,. \tag{16}$$

For stationary flow, Wilson (1987) proposed $\Lambda = 10$ whereas Sumer et al. (1996) found $\Lambda = 11.8$. Different values for the peak sheet layer thickness under oscillatory flow were proposed ranging from 13 to 35. (e.g., Dohmen-Janssen et al. 2001; Dong et al. 2013).

The bed shear stress τ_b is commonly expressed by a quadratic drag law:

$$\tau_b = \frac{1}{2} f \rho_f U^2, \tag{17}$$

where f is a friction factor. The bed shear stress is difficult to determine directly in the swash zone and large uncertainties exist on the value of the friction factor (Hughes 1995; Puleo and Holland 2001; Conley and Griffin Jr 2004; Raubenheimer et al. 2004; Puleo et al. 2012). Since the mobility number does not depend on the friction factor, it was chosen to represent the hydrodynamic forcing in this study.

The correlation was calculated between mobilized sediment, represented by sheet thickness and sheet load, and hydrodynamic forcing, represented by the mobility number ψ. Sheet thickness was scaled by d_{50}, similar to previous predictions of sheet thickness as a function of hydrodynamic forcing (16), and sheet load was scaled by $d_{50}\rho_s$. During sampling instances when more than one CCP captured the sheet flow layer, the mean of the sheet thicknesses and sheet load measurements from both instruments was used so that a single sampling instance is only counted once in the correlation. Scatter plots displayed in Fig. 6 show the sheet thickness (a) and sheet load (b) as a function of the mobility number.

The square of the Pearson correlation coefficient r^2 between sheet thickness and mobility number is 0.60, and the correlation coefficient between sheet load and mobility number is 0.53. The relationship between sheet thickness or sheet load and the mobility number was also assessed using a linear fit through the origin (solid line) similar to the linear relation between sheet thickness and Shields number (16) proposed by Wilson (1987). The resulting linear fits were:

$$\frac{\delta_s}{d_{50}} = 0.108\psi \tag{18}$$

$$\frac{C}{d_{50}\rho_s} = 0.0272\psi\,. \tag{19}$$

The root mean square errors of the linear fits through the origin were 10.2 for the sheet thickness and 2.81 for the sheet load. 73% of all profile measurements were within a factor of two of the fit through the origin (dashed lines) for the sheet thickness and 69% of all profile measurements for the sheet load. The

Journal of Waterway, Port, Coastal, and Ocean Engineering. Submitted November 28, 2012; accepted May 2, 2013; posted ahead of print May 4, 2013. doi:10.1061/(ASCE)WW.1943-5460.0000209

agreements between sheet thickness and mobility number and sheet load and mobility number are similar, because the sheet thickness determines the integration limits for the calculation of the sheet load, and thus calculated sheet thickness and sheet load are highly correlated ($r^2 = 0.96$).

Fig. 7 reprises the same time series excerpt as in Fig. 2 and shows time series of the measured mobility number, sheet thickness and sheet load. Sheet layer thickness exceeded 5 mm for five backwash events. Sheet thickness and sheet load typically increased monotonically during the backwash as the backwash velocity increased. Measurements at the end of backwash events when the flow depths became smaller than the elevation of the current meter indicate that the sheet thickness decreased at the end of the backwash, when flow velocities also decreased as bottom friction becomes dominant (e.g., at 17:31:01-17:31:07 UTC). In addition, uprush sheet flow events were also observed, e.g., at 17:30:47 UTC.

Sheet thickness and sheet load were also predicted by the linear fits (18) and (19). These values (orange crosses in Fig. 7 d-e) show that a prediction based on the mobility number alone reproduces the trend of increasing sheet thickness with increasing shear stress. The linear models generally underpredict measured sheet thickness and sheet load in the time excerpt shown. This is due to the fact that the linear fits are prescribed to intersect with the origin, and because sheet flows with a thickness less than 5 mm are not resolved by the CCP, as seen in the scatter plots in Fig. 6. Most measurements with $\delta_s \leq 11mm$ are underpredicted by the model (Fig. 6a), as sheet thickness measurements that were overpredicted would likely not be resolved by the CCP. Still, the linear fit through the origin provides the most adequate model for sheet thickness and sheet load because sheet flow layer thickness is zero when no hydrodynamic forcing is present and because it is supported by previous literature (Wilson 1987; Sumer et al. 1996). With root mean square errors of 8.93 for the sheet thickness and 3.14 for the sheet load for the time series excerpt displayed in Fig. 7, the agreement with the linear fit is representative for the entire dataset.

Discussion

The dataset presented here consists of 5365 individual sediment concentration profile measurements from a total of 423 sheet flow events, taken during three high tide cycles. Quality-controlled sheet flow with a sheet layer thickness exceeding 5 mm was recorded during 32 minutes out of 6.5 hours of measurements, meaning that a significant sheet flow layer was present for at least 8 % of the time and probably more, since sheet flow almost certainly also occurred during oblique flows and flows with a free surface level below the current meter that did not meet quality control criteria. This result demonstrates that significant sheet flow frequently occurs in the swash zone.

Backwash flows were deemed quasi-stationary when the measured flow acceleration was below a threshold of $1.2g\sin\gamma = 0.27m/s^2$. The analysis was repeated with an acceleration threshold reduced by a factor of four to $0.3g\sin\gamma = 0.07m/s^2$ to verify that flow accelerations below this threshold still had a negligible effect on the sheet flow. This lower threshold reduced the number of measurements that passed quality-control criteria from 3863 to 413. Fitting coefficients in the linear models for sheet thickness and

Journal of Waterway, Port, Coastal, and Ocean Engineering. Submitted November 28, 2012; accepted May 2, 2013; posted ahead of print May 4, 2013. doi:10.1061/(ASCE)WW.1943-5460.0000209

sheet load (18 – 19) changed by less than 2%, while the rmse errors for the fits decreased by 5% and 6% respectively. The small variations demonstrate that flow acceleration effects were indeed negligible for the original threshold of $0.27 m/s^2$.

Backwash sheet flow when the water level was below the elevation of the lowest current meter could have been included in the analysis by estimating the depth-averaged velocity using a continuity technique (Blenkinsopp et al. 2010, 2011a). A LiDAR scanner and an array of ultrasonic distance meters (UDMs) that are capable of generating an estimate of the depth-averaged velocity were deployed during the field study. However, only velocity measurements by the electromagnetic current meters were used in the present study because combining velocity measurements from different instruments could provide an additional source of variability in the dataset, and this may obfuscate the relationship between the sheet flow layer thickness and hydrodynamic forcing.

Besides during the backwash, sheet flow was also observed during the uprush, e.g., at 17:30:46 - 17:30:48 UTC in Fig. 7. Sheet flow during uprush is more difficult to analyze than quasi-steady backwash sheet flow since it is influenced by additional forcing mechanisms such as bore-generated turbulence, pressure gradients and phase lags. For this reason, this study focused on sheet flow during quasi-steady backwash conditions.

The sheet flow sediment concentration profile has a linear shape in the lower section of the sheet layer and a power law shape in the upper section of the sheet layer, with the transition between the two shapes occurring at sediment concentrations of 0.20-0.30. The profile is also self-similar for different sheet layer thicknesses. A linear shape, assumed by some sheet flow sediment transport models such as Hanes and Bowen (1985) and Wilson (1987), is in poor agreement with measured concentration profiles. A curve that incorporates the linear and power law, such as a composite profile or the empirical curve by O'Donoghue and Wright (2004a), is in excellent agreement with the field observations.

Adopting a curve such as the combined linear and power law or the empirical curve by O'Donoghue and Wright (2004a) can lead to improved sheet flow sediment transport models. For example, Wilson (1987) provided an analytical derivation of the sheet thickness by assuming that the bed shear stress τ_b at the bottom of the sheet layer is balanced by an intergranular shear stress, expressed as a Coulomb failure criterion:

$$\tau_b = \sigma_s \tan\phi' \ , \tag{20}$$

where ϕ' is the dynamic friction angle of the solids and σ_s is the intergranular normal stress:

$$\sigma_s = \int_{z_e}^{z_t} \rho_f g (s-1) c(z) dz \ . \tag{21}$$

Wilson (1987) assumed a linear concentration profile $c(z)$ in the sheet layer and a sediment concentration of zero at the top of the sheet layer, yielding:

Journal of Waterway, Port, Coastal, and Ocean Engineering. Submitted November 28, 2012; accepted May 2, 2013; posted ahead of print May 4, 2013. doi:10.1061/(ASCE)WW.1943-5460.0000209

$$\sigma_s = \rho_f g\left(s-1\right)\frac{\delta_s}{2}c_b \ . \tag{22}$$

Combining (20) and (22) yields

$$\frac{\delta_s}{d} = \frac{2}{c_b \tan\phi'}\frac{\tau_b}{\rho_f g\left(s-1\right)d} = \frac{2}{c_b \tan\phi'}\theta = \Lambda\theta \ . \tag{23}$$

Wilson (1987) assumed $c_b = 0.625$ and $\tan\phi' = 0.32$, leading to $\Lambda = 10$. Assuming a linear law with a power-law tail at the top of the sheet flow layer instead leads to higher values for Λ. For example, evaluating σ_s using the ODW curve with $\alpha = 1.73$ (12) and assuming $c_t = 0.08$ at the top of the sheet layer leads to $\Lambda = 11.8$, the same value as found by Sumer et al. (1996). The exact value of Λ is also influenced by assumptions on the sediment concentration in the bed c_b and the dynamic friction angle ϕ', but the improved description of the shape of the concentration profile nevertheless leads to sheet thickness estimates that are in better agreement with previous measurements.

Sheet thickness has previously been predicted as a linear function of the Shields number (16). Because of the difficulty in determining the bottom shear stress in the swash zone, sheet thicknesses and sheet load were related to the mobility number ψ in this study. The mobility number ψ can be related to the Shields number θ when a constant friction factor is assumed:

$$\theta = \frac{1}{2}f\psi \ , \tag{24}$$

By using (24), the linear fit between mobility number and the sheet flow layer thickness based on the dataset analyzed in this study is equivalent to the linear law based on the Shields number (16) with $\kappa = 11.8$ (Sumer et al. 1996) when a friction factor $f = 0.018$ is assumed. Velocity profile measurements in the bottom boundary layer during high tide 7, assuming a logarithmic velocity profile, yielded $f = 0.021 \pm 0.012$ during backwash flows (Puleo et al. this issue). The small difference between the friction factor estimates indicates that the sheet thickness measurements found here are in good agreement with past predictions based on the Shields number. This result, however, does not contravene the fact that there is still significant scatter associated with field measurements of bed shear stress, friction factors and sheet flow layer thicknesses in the swash zone, as illustrated by the scatter in Fig. 6 for sheet layer thickness and the standard deviation in the friction factor estimate based on velocity measurements. Additionally, sheet thickness values may vary between different studies because they were based on different measurement techniques, e.g. concentration measurements (e.g., Sumer et al. 1996; Dohmen-Janssen and Hanes 2005, this study) or visual methods (e.g., Dong et al. 2013) or because they were based on different definitions for the top and bottom boundary of the sheet flow layer.

Journal of Waterway, Port, Coastal, and Ocean Engineering. Submitted November 28, 2012; accepted May 2, 2013; posted ahead of print May 4, 2013. doi:10.1061/(ASCE)WW.1943-5460.0000209

Laboratory measurements have shown that sheet flow initiates above a threshold Shields number of 0.5 – 1.0 (Nielsen 1992; Asano 1995) or a threshold mobility number of approx. 240 (Dingler and Inman 1976). Including a threshold value in the linear models (18 – 19), similar to the threshold value in the bedload transport formula by Meyer-Peter and Müller (1948), could therefore yield a more accurate representation of the relationship between sheet thickness, sheet load and the mobility number. A threshold value was not included in the linear models (18 – 19) to facilitate comparison with existing relationships between sheet thickness and bed shear stress that also do not include a threshold value, such as the relationships proposed by Wilson (1987) and Sumer et al. (1996). In addition, accurately resolving a threshold value would require measurements of small sheet thicknesses near the threshold but these were not resolved by the sensor.

Sheet load magnitudes of up to 14 kg/m^2 were frequently observed during quasi-steady backwash events. Suspended loads of up to 4 kg/m^2 were observed in a preliminary analysis of fiber-optic backscatter sensor (FOBS) measurements during high tide 7 and were typically O(1-10) times smaller than concurrent sheet load magnitudes (Puleo et al. this issue), indicating that near-bed sediment loads are not negligible in the swash zone. More important than the sediment loads, however, are the sediment fluxes (sediment concentration multiplied by sediment velocity) and depth-integrated sediment transport but these require knowledge of the velocity profile in the sheet layer. The velocity profile in the sheet layer has been measured in laboratory experiments, e.g., using image analysis through the side-wall of a flow tunnel (Ahmed and Sato 2001; Capart et al. 2002), using an in-situ boroscope (Cowen et al. 2010) or by computing the cross-correlation of sediment concentration time series measured at different locations along the flow (McLean et al. 2001). Acoustic Doppler velocimetry techniques have been optimized to penetrate into the sheet layer, but it is unsure if measurements can be made at high concentrations in the lower sections of the sheet layer (Hurther et al. 2011). None of these techniques are readily deployable in the field, either because the measurement instruments cannot be deployed without generating significant flow disturbance and scour, or because repeatable, controllable conditions are required to obtain reliable velocity estimates. In the absence of measurement techniques to directly record sediment velocities in the sheet layer under field conditions, a velocity profile could be extrapolated down from current meter measurements higher in the water column to the non-moving sediment bed to obtain a sediment transport estimate, e.g., using analytical models such as Hanes and Bowen (1985) or numerical models such as Yu et al. (2010). Flow velocities in the sheet flow layer are smaller than in the suspended load layer due to bottom friction, meaning that the ratio between sheet flow sediment transport and suspended load transport is smaller than the ratio between sheet load and suspended load (Puleo et al. this issue).

Conclusions

Sediment concentration profiles in the sheet flow layer were measured in the swash zone of a dissipative beach using three conductivity concentration profilers, providing the first detailed measurements of sheet flow under field conditions. This paper focused on sheet flow during quasi-steady backwash conditions when the effects of surface-generated turbulence, phase lags and pressure gradients on the sheet flow layer were negligible, simplifying the hydrodynamic forcing for the sheet flow. From 6.5 hours of measurements

Journal of Waterway, Port, Coastal, and Ocean Engineering. Submitted November 28, 2012; accepted May 2, 2013; posted ahead of print May 4, 2013. doi:10.1061/(ASCE)WW.1943-5460.0000209

spanning three high tides, 16 minutes of sheet flow was recorded during quality controlled, quasi-steady backwash conditions, providing a dataset of 5365 instantaneous sediment concentration profiles.

The concentration profiles were grouped according to sheet flow layer thickness and ensemble-averaged. The sheet flow sediment concentration profile has a linear shape in the lower section and a power-law shape in the upper section, with the transition between the two shapes occurring at sediment volume fractions of 0.20-0.30. The profile shape is self-similar for sediment concentration profiles of varying sheet thicknesses ranging from 6 mm to 18 mm and can be described by a curve based on O'Donoghue and Wright (2004a). Adopting this curve as the sediment concentration profile provides an improvement to the analytical model for sheet flow layer thickness developed by Wilson (1987). This linear-power law curve shape also has significance toward future models of nearbed sediment transport where the sediment concentration profile in the sheet flow layer requires parameterization.

The sheet flow layer thickness and sheet load are well-correlated to the hydrodynamic forcing represented by the mobility number ψ, with $r^2 = 0.60$ for the sheet layer thickness and $r^2 = 0.53$ for the sheet load. A simple model with the nondimensional sheet thickness and sheet load proportional to the mobility number provides a good prediction of a time series of sheet thickness and sheet load.

Acknowledgements

This work was supported by the National Science Foundation under Grant No. OCE-0845004. Additional support for this work was provided by the University of Delaware, the Delaware Department of Natural Resources and Environmental Control, the Award for Global Research, Internships, and Performances for Graduate Students at the University of Delaware, the Natural Environmental Research Council, the US-UK Fulbright Commission and the Australian Research Council (DP110101176). The authors would like to thank D. Buscombe, T. Poate, R. McCall, B. Proença, L. Melo De Almeida, M. Sheridan, and P. Ganderton for their assistance with the field measurements and three anonymous reviewers for their valuable comments that improved this manuscript.

References

Ahmed, A. S. M., and Sato, S. (2001). "Investigation of bottom boundary layer dynamics of movable bed by using enhanced PIV technique." *Coast. Eng. J.*, 43(04), 239–258.

Ahmed, A. S. M., and Sato, S. (2003). "A Sheetflow Transport Model for Asymmetric Oscillatory Flows: Part II: Mixed Grain Size Sediments." *Coast. Eng. J.*, 45(03), 339–361.

Amoudry, L., Hsu, T.-J., and Liu, P. L.-F. (2008). "Two-phase model for sand transport in sheet flow regime." *J. Geophys. Res.*, 113(C3), C03011.

Journal of Waterway, Port, Coastal, and Ocean Engineering. Submitted November 28, 2012; accepted May 2, 2013; posted ahead of print May 4, 2013. doi:10.1061/(ASCE)WW.1943-5460.0000209

Archie, G. (1942). "The electrical resistivity log as an aid in determining some reservoir characteristics." *Inst. Mining Metall. Trans*, 146, 54–62.

Asano, T. (1995). "Sediment transport under sheet-flow conditions." *J. Waterw. Port Coast. Ocean Eng.*, 121, 239–246.

Bagnold, R. A. (1954). "Experiments on a Gravity-Free Dispersion of Large Solid Spheres in a Newtonian Fluid under Shear." *Proc. R. Soc. Lond. A*, 225(1160), 49–63.

Bagnold, R. A. (1956). "The Flow of Cohesionless Grains in Fluids." *Proc. R. Soc. Lond. Ser. A Math. Phys. Sci.*, 249(964), 235–297.

Bagnold, R. A. (1966). "The shearing and dilatation of dry sand and the 'singing' mechanism." *Proc. R. Soc. Lond. Ser. A Math. Phys. Sci.*, 295(1442), 219–232.

Baker, J., and Kudrolli, A. (2010). "Maximum and minimum stable random packings of Platonic solids." *Phys. Rev. E*, 82(6), 061304.

Bakhtyar, R., Yeganeh-Bakhtiary, A., Barry, D. A., and Ghaheri, A. (2009). "Two-phase hydrodynamic and sediment transport modeling of wave-generated sheet flow." *Adv. Water Resour.*, 32(8), 1267–1283.

Bakker, W. T., Van Kesteren, W. G. M., and Yu, Z. H. (1988). "Grain-Grain Interaction in Oscillating Sheetflow." *Proc. 21st Int. Conf. Coastal Eng*, ASCE, Torremolinos, Spain, 718–731.

Blenkinsopp, C. E., Mole, M. A., Turner, I. L., and Peirson, W. L. (2011a). "Measurements of the time-varying free-surface profile across the swash zone obtained using an industrial LIDAR." *Coast. Eng.*, 57(11-12), 1059–1065.

Blenkinsopp, C. E., Turner, I. L., Masselink, G., and Russell, P. E. (2010). "Validation of volume continuity method for estimation of cross-shore swash flow velocity." *Coast. Eng.*, 57(10), 953–958.

Blenkinsopp, C. E., Turner, I. L., Masselink, G., and Russell, P. E. (2011b). "Swash zone sediment fluxes: Field observations." *Coast. Eng.*, 58(1), 28–44.

Butt, T., and Russell, P. (1999). "Suspended sediment transport mechanisms in high-energy swash." *Mar. Geol.*, 161(2-4), 361–375.

Journal of Waterway, Port, Coastal, and Ocean Engineering. Submitted November 28, 2012; accepted May 2, 2013; posted ahead of print May 4, 2013. doi:10.1061/(ASCE)WW.1943-5460.0000209

Cáceres, I., and Alsina, J. M. (2012). "A detailed, event-by-event analysis of suspended sediment concentration in the swash zone." *Cont. Shelf Res.*, 41(0), 61–76.

Calantoni, J., and Puleo, J. A. (2006). "Role of pressure gradients in sheet flow of coarse sediments under sawtooth waves." *J. Geophys. Res.*, 111(C1), C01010.

Capart, H., and Fraccarollo, L. (2011). "Transport layer structure in intense bed-load." *Geophys. Res. Lett.*, 38(20), L20402.

Capart, H., Young, D. L., and Zech, Y. (2002). "Voronoï imaging methods for the measurement of granular flows." *Exp. Fluids*, 32(1), 121–135.

Chen, X., Li, Y., Niu, X., Chen, D., and Yu, X. (2011). "A two-phase approach to wave-induced sediment transport under sheet flow conditions." *Coast. Eng.*, 58(11), 1072 – 1088.

Conley, D. C., and Griffin Jr, J. G. (2004). "Direct measurements of bed stress under swash in the field." *J. Geophys. Res.*, 109(C3), C03050.

Cowen, E., Dudley, R., Liao, Q., Variano, E., and Liu, P. (2010). "An insitu borescopic quantitative imaging profiler for the measurement of high concentration sediment velocity." *Exp. Fluids*, 49(1), 77–88.

Dibajnia, M., and Watanabe, A. (1998). "Transport rate under irregular sheet flow conditions." *Coast. Eng.*, 35(3), 167–183.

Dingler, J. R., and Inman, D. L. (1976). "Wave-Formed Ripples in Nearshore Sands." *Proc. 15th Int. Conf. Coastal Eng*, ASCE, Honolulu, HI, 2109–2126.

Dohmen-Janssen, C. M., and Hanes, D. M. (2002). "Sheet flow dynamics under monochromatic nonbreaking waves." *J. Geophys. Res.*, 107(C10), 21.

Dohmen-Janssen, C. M., and Hanes, D. M. (2005). "Sheet flow and suspended sediment due to wave groups in a large wave flume." *Cont. Shelf Res.*, 25(3), 333–347.

Dohmen-Janssen, C. M., Hassan, W. N., and Ribberink, J. S. (2001). "Mobile-bed effects in oscillatory sheet flow." *J. Geophys. Res.*, 106(C11), PP. 27,103–27,115.

Dong, L. P., Sato, S., and Liu, H. (2013). "A sheetflow sediment transport model for skewed-asymmetric waves combined with strong opposite currents." *Coast. Eng.*, 71(0), 87–101.

Journal of Waterway, Port, Coastal, and Ocean Engineering. Submitted November 28, 2012; accepted May 2, 2013; posted ahead of print May 4, 2013. doi:10.1061/(ASCE)WW.1943-5460.0000209

Foster, D. L., Bowen, A. J., Holman, R. A., and Natoo, P. (2006). "Field evidence of pressure gradient induced incipient motion." *J. Geophys. Res.*, 111(C05), C05004.

Hanes, D. M., and Bowen, A. J. (1985). "A granular-fluid model for steady intense bed-load transport." *J. Geophys. Res.*, 90(C5), 9149–9158.

Hanes, D. M., and Inman, D. L. (1985). "Observations of rapidly flowing granular-fluid materials." *J. Fluid Mech.*, 150, 357–380.

Horikawa, K., Watanabe, A., and Katori, S. (1982). "Sediment transport under sheet flow conditions." *Proc. 18th Int. Conf. Coastal Eng*, Cape Town, South Africa, 1335–1352.

Hsu, T.-J., Jenkins, J. T., and Liu, P. L.-F. (2004). "On two-phase sediment transport: sheet flow of massive particles." *Proc. R. Soc. Lond. Ser. A Math. Phys. Sci.*, 460(2048), 2223–2250.

Hughes, M. G. (1995). "Friction Factors for Wave Uprush." *J. Coast. Res.*, 11(4), 1089–1098.

Hughes, M. G., Aagaard, T., and Baldock, T. E. (2007). "Suspended Sediment in the Swash Zone: Heuristic Analysis of Spatial and Temporal Variations in Concentration." *J. Coast. Res.*, 23(6), 1345–1354.

Hughes, M. G., and Baldock, T. E. (2004). "Eulerian flow velocities in the swash zone: Field data and model predictions." *J. Geophys. Res.*, 109, C08009.

Hurther, D., Thorne, P. D., Bricault, M., Lemmin, U., and Barnoud, J.-M. (2011). "A multi-frequency Acoustic Concentration and Velocity Profiler (ACVP) for boundary layer measurements of fine-scale flow and sediment transport processes." 58(7), 594–605.

Lanckriet, T., Puleo, J. A., Masselink, G., Turner, I. L., Conley, D., Blenkinsopp, C., and Russell, P. (2012). "Field measurements of sheet flow sediment transport in the swash zone." *Proc. 33nd Int. Conf. Coastal Eng.*, ASCE, Valladolid, Spain.

Lanckriet, T., Puleo, J. A., and Waite, N. (2013). "A Conductivity Concentration Profiler for Sheet Flow Sediment Transport." *IEEE J. Ocean. Eng.*, 38(1), 55 –70.

Masselink, G., Evans, D., Hughes, M. G., and Russell, P. (2005). "Suspended sediment transport in the swash zone of a dissipative beach." *Mar. Geol.*, 216(3), 169–189.

Masselink, G., and Puleo, J. A. (2006). "Swash-zone morphodynamics." *Cont. Shelf Res.*, 26(5), 661–680.

Journal of Waterway, Port, Coastal, and Ocean Engineering. Submitted November 28, 2012; accepted May 2, 2013; posted ahead of print May 4, 2013. doi:10.1061/(ASCE)WW.1943-5460.0000209

McLean, S. R., Ribberink, J. S., Dohmen-Janssen, C. M., and Hassan, W. N. (2001). "Sand Transport in Oscillatory Sheet Flow with Mean Current." *J. Waterw. Port Coast. Ocean Eng.*, 127(3), 141–151.

Meyer-Peter, E., and Müller, R. (1948). "Formulas for bed-load transport." Proceedings of the 2nd Meeting of the International Association for Hydraulic Structures Research, Stockholm, 39–64.

Nielsen, P. (1992). *Coastal bottom boundary layers and sediment transport*. Advanced Series on Ocean Engineering, World Scientific, Singapore.

O'Donoghue, T., and Wright, S. (2004a). "Concentrations in oscillatory sheet flow for well sorted and graded sands." *Coast. Eng.*, 50(3), 117–138.

O'Donoghue, T., and Wright, S. (2004b). "Flow tunnel measurements of velocities and sand flux in oscillatory sheet flow for well-sorted and graded sands." *Coast. Eng.*, 51(11-12), 1163–1184.

Osborne, P. D., and Rooker, G. A. (1999). "Sand Re-Suspension Events in a High Energy Infragravity Swash Zone." *J. Coast. Res.*, 15(1), 74–86.

Pugh, F. J., and Wilson, K. C. (1999). "Velocity and concentration distributions in sheet flow above plane beds." *J. Hydraul. Eng.*, 125(2), 117–125.

Puleo, J. A., Beach, R. A., Holman, R. A., and Allen, J. S. (2000). "Swash zone sediment suspension and transport and the importance of bore-generated turbulence." *J. Geophys. Res.*, 105(C7), 17021–17044.

Puleo, J. A., Blenkinsopp, C., Conley, D., Masselink, G., Turner, I. L., Russell, P., Buscombe, D., Howe, D., Lanckriet, T., McCall, R., and Poate, T. (this issue). "A comprehensive field study of swash-zone processes, Part 1: Experimental design with examples of hydrodynamic and sediment transport measurements." *J. Waterw. Port Coast. Ocean Eng.*

Puleo, J. A., and Holland, K. T. (2001). "Estimating swash zone friction coefficients on a sandy beach." *Coast. Eng.*, 43(1), 25–40.

Puleo, J. A., Lanckriet, T., and Wang, P. (2012). "Near bed cross-shore velocity profiles, bed shear stress and friction on the foreshore of a microtidal beach." *Coast. Eng.*, 68(0), 6–16.

Raubenheimer, B., Elgar, S., and Guza, R. T. (2004). "Observations of swash zone velocities: A note on friction coefficients." *J. Geophys. Res.*, 109(C1), C01027.

Journal of Waterway, Port, Coastal, and Ocean Engineering. Submitted November 28, 2012; accepted May 2, 2013; posted ahead of print May 4, 2013. doi:10.1061/(ASCE)WW.1943-5460.0000209

Ribberink, J. S., and Al-Salem, A. A. (1994). "Sediment transport in oscillatory boundary layers in cases of rippled beds and sheet flow." *J. Geophys. Res.*, 99(C6), 12707–12,727.

Ribberink, J. S., and Al-Salem, A. A. (1995). "Sheet flow and suspension of sand in oscillatory boundary layers." *Coast. Eng.*, 25(3-4), 205–225.

Ribberink, J. S., van der Werf, J. J., O'Donoghue, T., and Hassan, W. N. M. (2008). "Sand motion induced by oscillatory flows: Sheet flow and vortex ripples." *J. Turbul.*, 9(20), 1–32.

Ruessink, B. G., Michallet, H., Abreu, T., Sancho, F., A, D. A. V. der, Werf, J. J. V. der, and Silva, P. A. (2011). "Observations of velocities, sand concentrations, and fluxes under velocity-asymmetric oscillatory flows." *J. Geophys. Res.*, 116(C3), C03004.

Savage, S. B., and Mckeown, S. (1983). "Shear stresses developed during rapid shear of concentrated suspensions of large spherical particles between concentric cylinders." *J. Fluid Mech.*, 127, 453–472.

Schretlen, J. J. L. M., Ribberink, J. S., and O'Donoghue, T. (2010). "Boundary layer flow and sand transport under full scale surface waves." *Proc. 32nd Int. Conf. Coastal Eng.*, ASCE, Shanghai, China.

Shook, C., Gillies, R., Haas, D., Husband, W., and Small, M. (1982). "Flow of coarse and fine sand slurries in pipelines." *J. Pipelines*, 3(1), 13–21.

Sleath, J. F. A. (1999). "Conditions for plug formation in oscillatory flow." *Cont. Shelf Res.*, 19(13), 1643–1664.

Song, C., Wang, P., and Makse, H. A. (2008). "A phase diagram for jammed matter." *Nature*, 453(7195), 629–632.

Sumer, B. M., Kozakiewicz, A., Fredsoe, J., and Deigaard, R. (1996). "Velocity and Concentration Profiles in Sheet-Flow Layer of Movable Bed." *J. Hydraul. Eng.*, 122(10), 549–558.

Van der A, D. A., O'Donoghue, T., and Ribberink, J. S. (2010). "Measurements of sheet flow transport in acceleration-skewed oscillatory flow and comparison with practical formulations." *Coast. Eng.*, 57(3), 331–342.

Wilson, K. C. (1987). "Analysis of Bed-Load Motion at High Shear Stress." *J. Hydraul. Eng.*, 113(1), 97–103.

Yu, X., Hsu, T.-J., and Hanes, D. M. (2010). "Sediment transport under wave groups: Relative importance between nonlinear waveshape and nonlinear boundary layer streaming." *J. Geophys. Res.*, 115(C2), C02013.

Journal of Waterway, Port, Coastal, and Ocean Engineering. Submitted November 28, 2012; accepted May 2, 2013; posted ahead of print May 4, 2013. doi:10.1061/(ASCE)WW.1943-5460.0000209

Yu, X., Hsu, T.-J., Jenkins, J. T., and Liu, P. L.-F. (2012). "Predictions of vertical sediment flux in oscillatory flows using a two-phase, sheet-flow model." *Adv. Water Resour.*, 48(0), 2–17.

Yu, Z., Niemeyer, H. D., and Bakker, W. T. (1990). "Site investigation on sand concentration in the sheet-flow layer." *Proc. 22nd Int. Conf. Coastal Eng.*, ASCE, Delft, The Netherlands, 2361–2371.

Journal of Waterway, Port, Coastal, and Ocean Engineering. Submitted November 28, 2012; accepted May 2, 2013; posted ahead of print May 4, 2013. doi:10.1061/(ASCE)WW.1943-5460.0000209

Figures

Fig. 1. Sideways view of three buried CCPs, indicated by arrows. Down-hanging probes are Vectrino-II velocimeters. Yellow tape measure indicates scale.

Fig. 2. Time series excerpt of swash-zone measurements. (a) Water depth. (b) Cross-shore (solid line) and alongshore (dotted line) velocity. Thick black line indicates when quasi-steady backwash sheet flow occurred that complied with all quality-control criteria. (c) Sediment volume fraction measured by CCP. Magenta (black) line indicates top (bottom) of sheet layer, yellow vertical lines indicate times when instantaneous profiles are displayed in panels d-g. (d-g) Instantaneous sediment volume fraction profiles measured by two collocated CCPs during four instances of the event, indicated by yellow lines in panel c.

Fig. 3. Instantaneous sediment concentration profiles recorded during quasi-steady backwash events at (a) 17:30:15.75 UTC (Fig. 2d) and (b) 17:32:1.50 UTC (Fig. 2g). Black line indicates the measured concentration profile. Blue line indicates curve fit of the form eq. (4). Red diamond indicates inflection point in curve. Red upward facing triangle and red downward-facing triangle indicate the top and bottom of the sheet layer, z_t and z_e, respectively.

Fig. 4. Ensemble-averaged sediment concentration profiles for sheet thicknesses of 6 mm (left column), 11 mm (middle column) and 16 mm (right column). Gray lines indicate individual profiles; dotted black line indicates ensemble-averaged profile. Horizontal lines indicate top and bottom of sheet layer. Top row: Orange solid line indicates linear fit. Middle row: blue solid line and orange dashed line indicate power law and linear law components of the composite curve fit. Bottom row: orange solid line indicates ODW curve with $\alpha = 1.73$ fixed.

Fig. 5. Individual sheet flow sediment concentration profiles normalized by sheet thickness. Black line indicates ensemble average of all normalized profiles, white dotted line indicates ODW curve with $\alpha = 1.73$.

Journal of Waterway, Port, Coastal, and Ocean Engineering. Submitted November 28, 2012; accepted May 2, 2013; posted ahead of print May 4, 2013. doi:10.1061/(ASCE)WW.1943-5460.0000209

Fig. 6 (a) Sheet flow thickness δ_s as a function of mobility number ψ, (b) Sheet load C as a function of mobility number ψ. Solid line indicates best fit through origin; dashed lines indicate factor two range. No measurements are displayed with sheet layer thicknesses less than 5 mm as they cannot be resolved by the CCP.

Fig. 7. Time series excerpt of swash zone measurements. (a) Water depth. (b) Cross-shore (solid line) and alongshore (dashed line) velocity. (c) Mobility number. Thick black lines in panels b and c indicate times when quasi-steady backwash sheet flow occurred. (d) Sheet thickness and (e) sheet load. Black dots indicate measurements during quasi-steady backwash, gray dots indicate measurements during uprush sheet flow events that met quality control criteria and during backwash sheet flow events when no current meter data was available. Orange crosses indicate predictions by fits through origin (eq. 18-19).

Tables

Table 1. Wave and tidal conditions during the high tide measurement periods. Start and end times for high tides are based on the first and last swash event registered by a buried pressure transducer at the main instrument rig.

Tide number	Time	High tide level (m Ordnance Datum Newlyn)	H_s (m)	T_p (s)	u_{max} (m/s) (uprush)	u_{min} (m/s) (backwash)
7	October 13 2011, 16:16 – 18:57 UTC	3.10	1.22	10.9	2.21	-2.19
8	October 14 2011, 04:40 – 07:13 UTC	3.06	0.96	10.5	2.35	-1.98
9	October 14 2011, 17:03 – 19:18 UTC	3.01	0.64	9.6	2.05	-1.79

Journal of Waterway, Port, Coastal, and Ocean Engineering. Submitted November 28, 2012; accepted May 2, 2013; posted ahead of print May 4, 2013. doi:10.1061/(ASCE)WW.1943-5460.0000209

Table 2. Summary of fitting results for ensemble-averaged profiles.

Sheet thickness (mm)	6	7	8	9	10	11	12	13	14	15	16	17	18
# profiles	1574	903	651	418	204	130	97	84	68	64	44	41	42
R^2: linear	0.97	0.96	0.96	0.97	0.96	0.96	0.94	0.92	0.92	0.90	0.89	0.87	0.87
R^2: power law	0.78	0.85	0.90	0.61	0.76	0.83	0.88	0.88	0.69	0.74	0.80	0.81	0.88
R^2: composite	0.99	1.00	1.00	1.00	1.00	1.00	1.00	1.00	1.00	1.00	1.00	1.00	1.00
$c_{transition}$	0.20	0.21	0.22	0.23	0.24	0.24	0.24	0.24	0.25	0.25	0.25	0.29	0.30
$z_{transition} / \delta_s$	0.57	0.54	0.51	0.48	0.46	0.44	0.43	0.39	0.38	0.36	0.35	0.27	0.28
R^2: ODW(α free)	0.98	0.99	0.99	0.99	0.99	0.99	1.00	1.00	1.00	1.00	1.00	1.00	1.00
α : ODW	2.03	1.99	1.94	1.89	1.86	1.82	1.80	1.65	1.61	1.56	1.53	1.44	1.51
R^2: ODW($\alpha = 1.73$)	0.95	0.97	0.97	0.98	0.99	0.99	1.00	0.99	0.99	0.98	0.98	0.94	0.96

Figure 1

Journal of Waterway, Port, Coastal, and Ocean Engineering. Submitted November 28, 2012; accepted May 2, 2013;
posted ahead of print May 4, 2013. doi:10.1061/(ASCE)WW.1943-5460.0000209

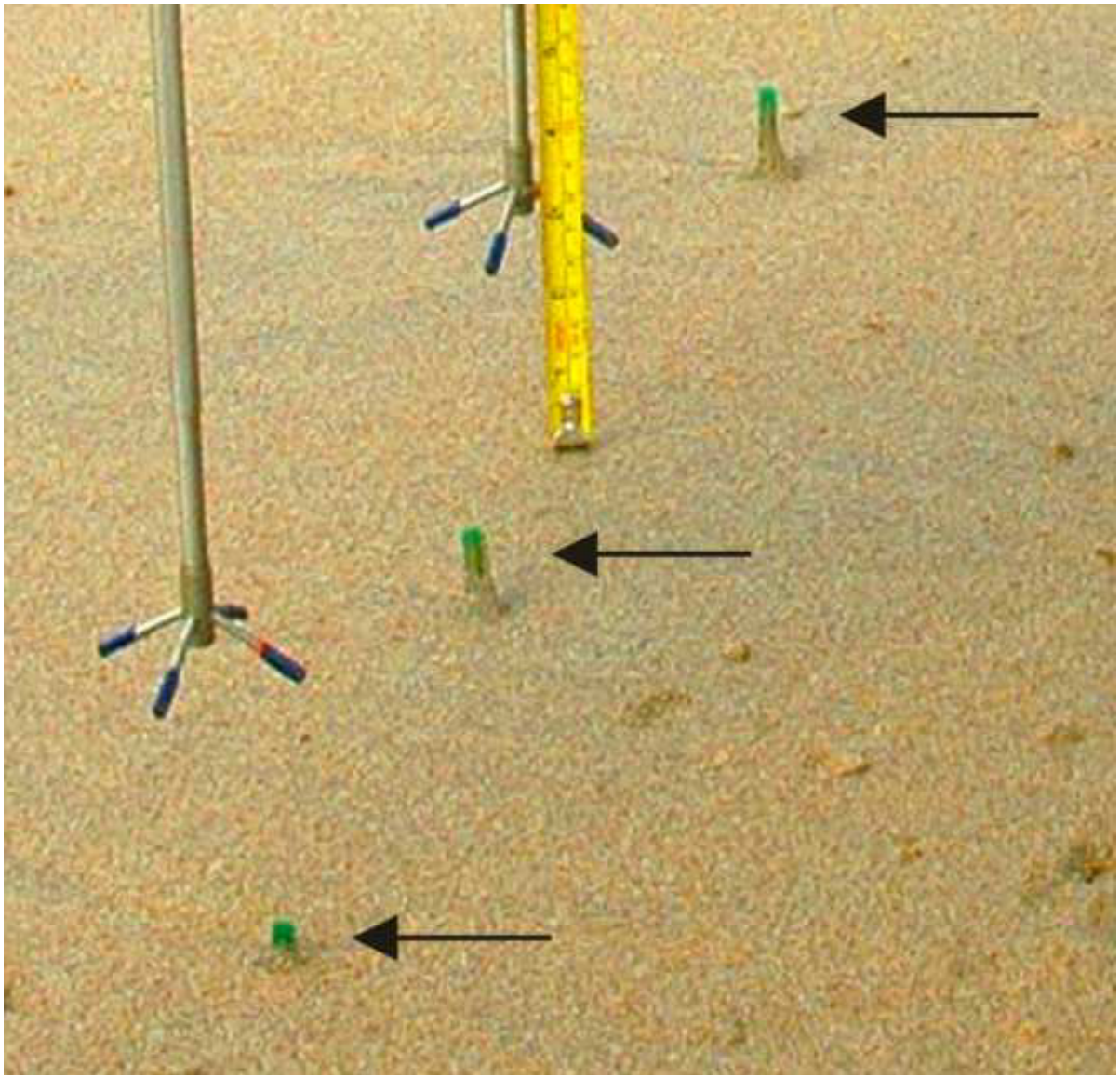

Journal of Waterway, Port, Coastal, and Ocean Engineering. Submitted November 28, 2012; accepted May 2, 2013;
posted ahead of print May 4, 2013. doi:10.1061/(ASCE)WW.1943-5460.0000209

Figure 2

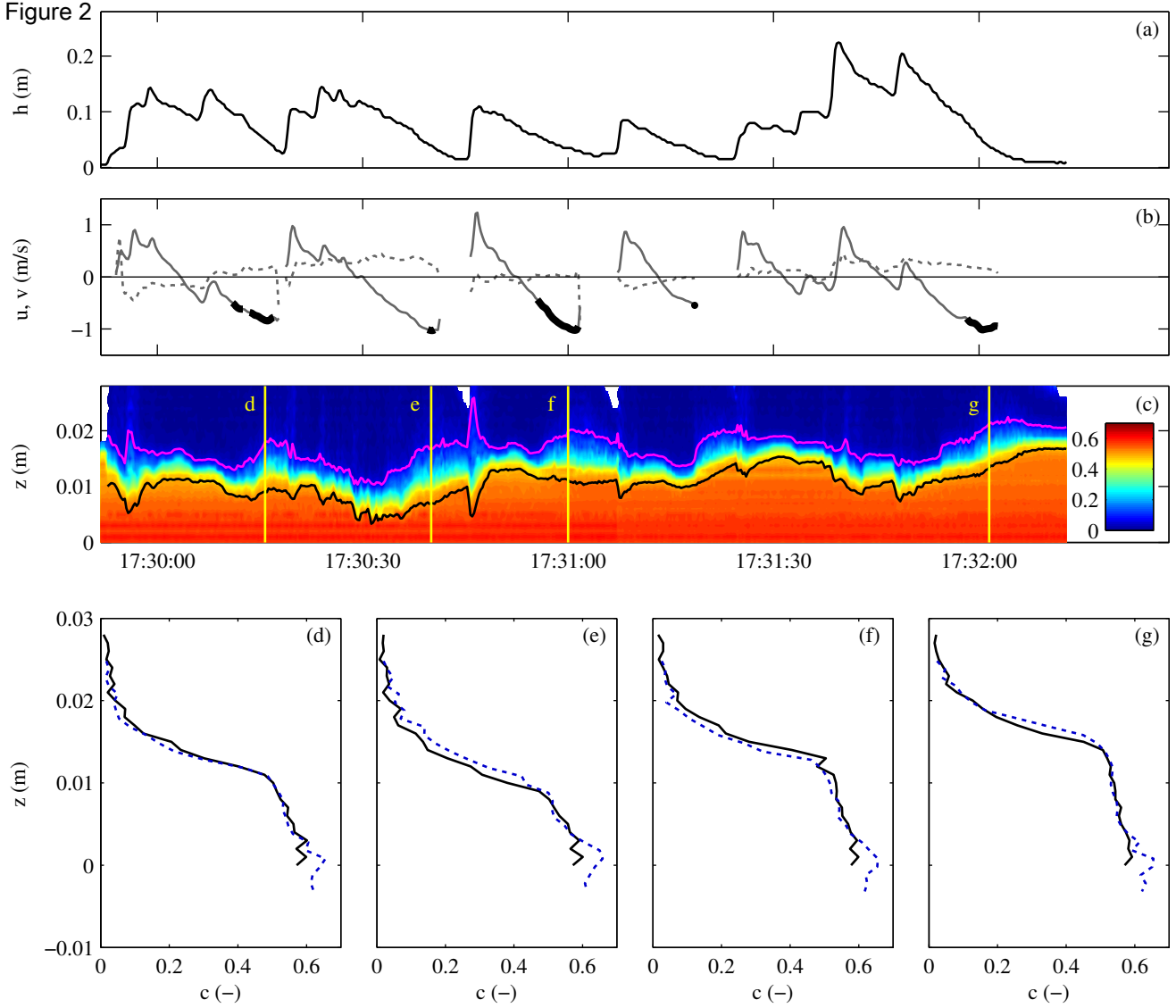

Figure 3

Journal of Waterway, Port, Coastal, and Ocean Engineering. Submitted November 28, 2012; accepted May 2, 2013; posted ahead of print May 4, 2013. doi:10.1061/(ASCE)WW.1943-5460.0000209

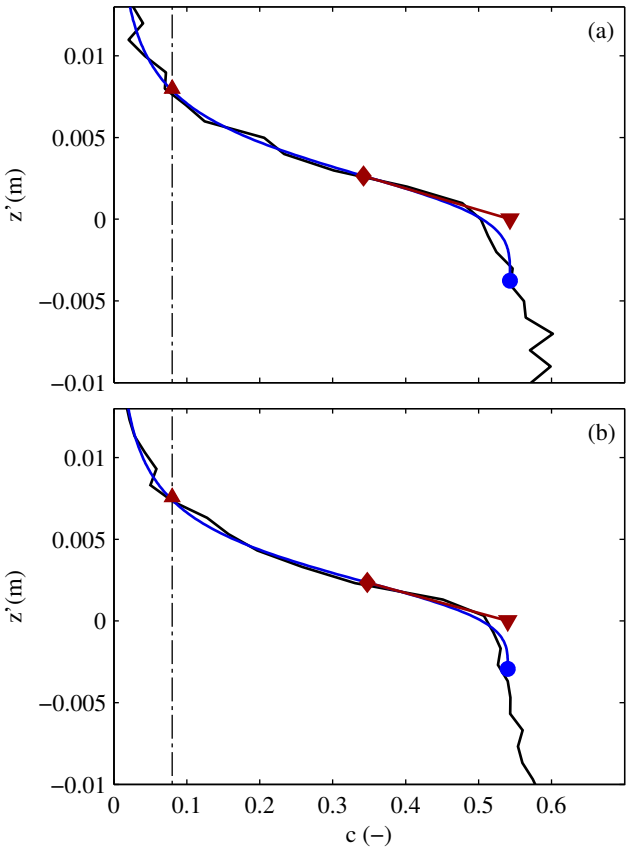

Figure 4

Journal of Waterway, Port, Coastal, and Ocean Engineering. Submitted November 28, 2012; accepted May 2, 2013;
posted ahead of print May 4, 2013. doi:10.1061/(ASCE)WW.1943-5460.0000209

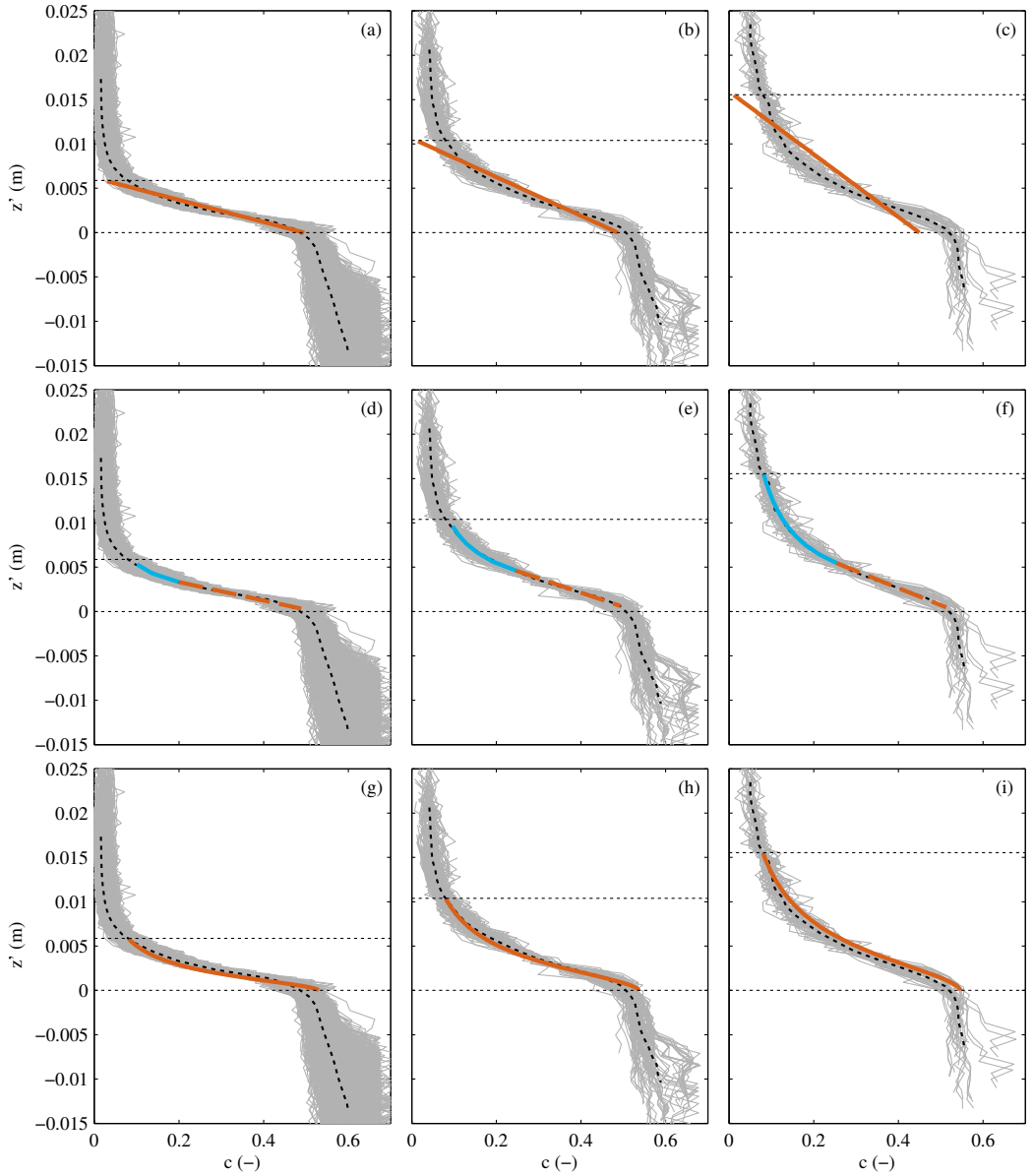

Figure 5

Journal of Waterway, Port, Coastal, and Ocean Engineering. Submitted November 28, 2012; accepted May 2, 2013; posted ahead of print May 4, 2013. doi:10.1061/(ASCE)WW.1943-5460.0000209

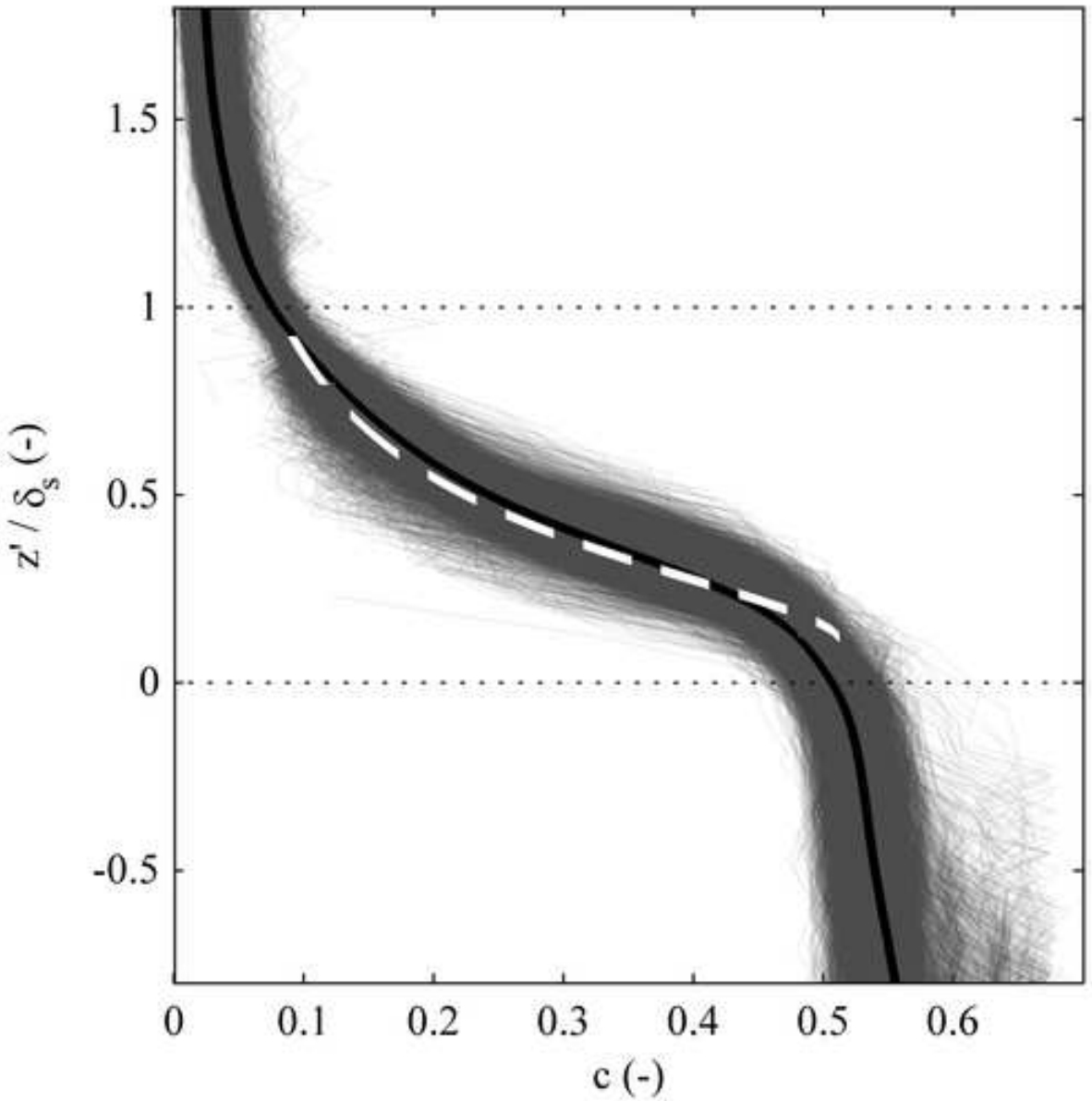

Figure 6

Journal of Waterway, Port, Coastal, and Ocean Engineering. Submitted November 28, 2012; accepted May 2, 2013;
posted ahead of print May 4, 2013. doi:10.1061/(ASCE)WW.1943-5460.0000209

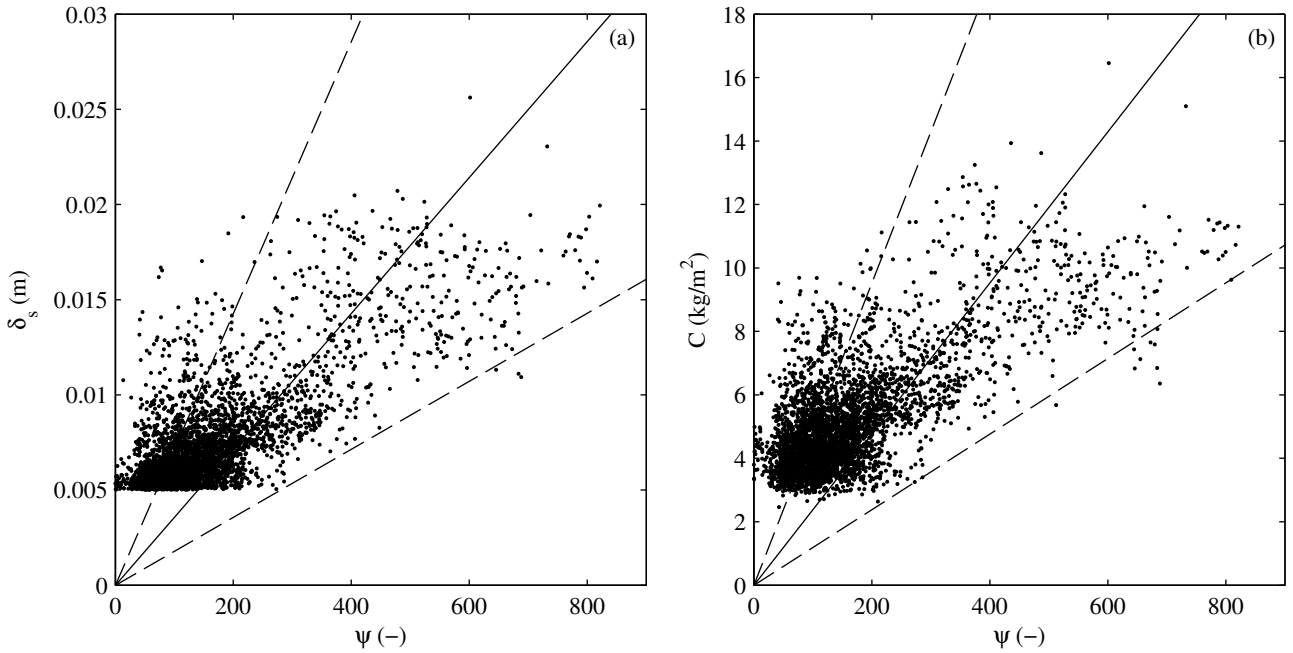

Figure 7

Journal of Waterway, Port, Coastal, and Ocean Engineering. Submitted November 28, 2012; accepted May 2, 2013;
posted ahead of print May 4, 2013. doi:10.1061/(ASCE)WW.1943-5460.0000209